

中国激光

功率 4.1 W, 脉宽 48 fs, 重复频率 74 MHz 的掺钛蓝宝石 飞秒激光振荡器

刘滋润^{1,2,3}, 陈兴进^{1,2,3}, 王楠^{1,2,3*}

¹ 深圳大学物理与光电工程学院, 广东深圳 518060;

² 深圳大学深圳市激光工程重点实验室, 广东深圳 518060;

³ 深圳大学光电子器件与系统教育部重点实验室, 广东深圳 518060

摘要 基于克尔透镜锁模机制, 实现了掺钛蓝宝石飞秒激光振荡器的高平均功率和短脉宽输出。使用功率为 16 W、波长为 532 nm 的连续光进行泵浦, 使用高折射率的棱镜对进行色散补偿, 同时使用狭缝辅助锁模, 实验获得了平均输出功率为 4.1 W、脉冲宽度为 48 fs、重复频率为 74.15 MHz 的飞秒脉冲。相比当前同类型激光器参数 (20 W 泵浦光下输出功率为 4 W, 脉宽为 130 fs, 重复频率为 76 MHz 的飞秒激光), 功率提升了 2.5%, 光-光转换效率提高了 28%, 脉宽缩短了 63%, 峰值功率提升了 2.8 倍。

关键词 激光器; 高平均功率; 克尔透镜锁模; 飞秒激光; 掺钛蓝宝石

中图分类号 TN248 文献标志码 A

DOI: 10.3788/CJL230501

1 引言

飞秒激光在激光微加工^[1-3]、生物医学双光子成像^[4]、外科手术^[5]、精密检测^[6]和飞秒化学^[7]等多个领域中具有实用价值。为了获得良好的光与物质相互作用的效果, 这些应用通常要求激光光源具有高功率和短脉宽的特性, 以获得更强的峰值功率或更好的时间分辨率。例如: 在非线性光学混频研究中, 高功率和短脉宽的基频光能提高谐波转换效率^[8-9]; 在双光子成像时, 高功率的光源有利于提高成像过程中的分辨率^[10]; 在多光子诱导半导体纳米粒子上转换光致发光研究中, 光致发光功率的增加与泵浦功率呈非线性正相关^[11-12]; 在使用超快泵浦-探测技术对金属或半导体材料进行非线性光学性质的测量时, 高功率的泵浦光源能提高激发材料产生的折射率、透射率或其他性质变化信号的强度^[13-15]。为了获得高功率的飞秒激光, 可以直接对单级激光振荡器进行锁模, 或利用啁啾脉冲放大(CPA)技术将低功率的种子激光放大。然而, 由于飞秒激光放大系统的结构复杂、造价昂贵, 单级高功率飞秒激光振荡器在特定情况下具有优势, 并且激光振荡器的脉冲重复频率通常在兆赫兹量级, 在应用中具有更高的脉冲作用效率。此外, 噗啾脉冲放大系统在脉冲对比度优化方面也对高功率的飞秒振荡器有一定要求^[16-18]。因此, 高平均功率、短脉冲宽度和高重复

频率的飞秒激光振荡器一直是超快激光器及其应用领域的研究热点之一。

由于具有超宽的发射光谱和较高的热导率, 掺钛蓝宝石是一种性能优良的飞秒激光器增益介质。Spence 等^[19]于 1991 年首次在钛宝石激光振荡器中获得了平均功率为 450 mW、脉冲宽度为 60 fs 的飞秒激光。之后 Huang 等^[20]、Proctor 等^[21]、Xu 等^[22]、Ell 等^[23]使用棱镜对、啁啾镜或二者组合作为腔内色散补偿装置, 钛宝石激光的脉冲宽度被不断压缩到亚 20 fs 至亚 10 fs 甚至两个光周期量级, 但是输出的平均功率仍维持在百毫瓦量级。由于存在着泵浦源的功率限制、热透镜效应和锁模脉冲的稳定性等问题, 钛宝石飞秒激光器的平均输出功率较难提升。为了提高钛宝石锁模激光输出的平均功率, Liu 等^[24]在腔内引入了连续光放大模块, 将激光器的输出功率提高到了 3.4 W, 脉冲宽度为 150 fs, 重复频率为 79 MHz。Naumov 等^[25]利用克尔透镜锁模机制, 在泵浦功率为 10 W 时获得了输出功率为 2.5 W、脉冲宽度为 50 fs、重复频率为 50 MHz 的激光输出。Dewald 等^[26]使用半导体可饱和吸收镜进行锁模, 在 15 W 的高功率泵浦下获得了输出功率为 3.5 W、脉冲宽度为 54 fs、重复频率为 6 MHz 的激光输出。最近, Takano 等^[27]将泵浦功率提高至 22.5 W, 在块材料钛宝石激光振荡器中获得了功率为 10 W 的连续激光输出。目前, 在商用高功率钛宝石飞秒激光振

收稿日期: 2023-02-08; 修回日期: 2023-03-06; 录用日期: 2023-03-21; 网络首发日期: 2023-03-31

基金项目: 深圳市科技创新项目(20200810161702001)、深圳市孔雀计划高端人才启动项目

通信作者: *nwang@szu.edu.cn

荡器产品中,相干公司生产的Mira系列在20 W的532 nm连续光泵浦下,能输出最高功率为4 W、脉冲宽度为130 fs、重复频率为76 MHz的飞秒脉冲^[28]。光谱物理公司生产的Tsunami系列在15 W的532 nm连续光泵浦下,能输出最高功率为2.7 W、脉冲宽度为100 fs、重复频率为80 MHz的飞秒脉冲^[29]。

通过腔内腰斑分析、色散仿真模型优化,并在两棱镜之间的光路中引入狭缝来控制激光光谱带宽和直流损耗,本文在自建的钛宝石激光振荡器中实现了平均功率为4.1 W、脉冲宽度为48 fs、重复频率为74.15 MHz的飞秒激脉冲输出。据我们所知,这是目前首次在钛宝石飞秒激光振荡器中直接获得平均功率大于4 W同时脉冲宽度小于50 fs的飞秒激光输出。

2 实验装置

本研究基于自建的常规钛宝石飞秒激光振荡器,使用4 W的532 nm连续光泵浦4 mm的钛宝石晶体,用熔融石英棱镜对补偿腔内色散,在透过率为7%的输出耦合镜下,获得了平均功率为500 mW、脉冲宽度为26 fs、重复频率为78 MHz的飞秒脉冲输出。当泵浦功率增加至5 W以上时,出现激光直流分量,锁模状态恶化。因此通过改变谐振腔参数,实现了图1所示的高功率克尔透镜锁模钛宝石飞秒振荡器。激光泵浦源为最大输出功率为16 W的532 nm连续光绿光激光

器。使用焦距为150 mm的平凸透镜将泵浦光聚焦到钛宝石晶体(尺寸为4 mm×4 mm×20 mm,吸收系数 $\alpha_{532}=2.23 \text{ cm}^{-1}$)中,晶体用钢箔包裹被安装在铜制水冷晶体架里。使用制冷功率为600 W的水冷机将水温控制在(14 ± 0.1)°C。C1和C2是一对曲率半径为150 mm、在750~850 nm光谱范围内高反的凹面镜,凹面镜折叠角(2θ)设置为24°。M1~M4均是在750~850 nm光谱范围内高反的平面镜。OC是透过率为20%的输出耦合镜。棱镜对P1、P2用于补偿腔内色散,其顶角间距设置为340 mm。激光谐振腔总长为2.02 m。不同于商用激光振荡器在端镜处放置狭缝以抑制高阶横模,本文在棱镜对之间的光路中放置一个可调狭缝,既能抑制腔内高阶横模,又可选择性地抑制腔内高功率激光运行时特定光谱处的直流分量。长焦距的透镜和长曲率半径的凹面镜使得泵浦光聚焦后的光斑束腰半径(经计算约为23 μm)与腔内激光束腰半径(经计算约为26 μm)相匹配,这不仅增大了激光束腰,避免高激光功率密度损伤晶体,还增加了激光模体体积,提高了输出功率^[30]。由于增益晶体较长,若选用低折射率的熔融石英棱镜对,则需要至少1700 mm的间距才能补偿腔内二阶色散(或群延迟色散,简称为GDD),因此选用了高折射率的棱镜,这样可用较短间距提供足量的负色散,并减小谐振腔所占空间。

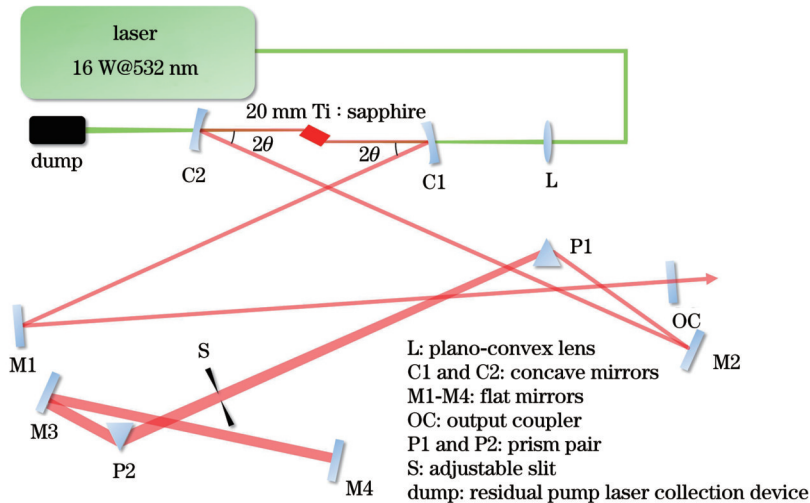


图1 钛宝石飞秒激光振荡器实验装置图

Fig. 1 Experimental device diagram of Ti:sapphire femtosecond oscillator

3 分析与讨论

基于ABCD矩阵^[31-32],凹面镜C2与钛宝石晶体的间距对谐振腔稳区分布的影响、谐振腔内光斑半径的分布以及折叠角与稳区的关系分别如图2(a)~(c)所示。调整谐振腔,使其工作在图2(a)所示的第二稳区(72.7~78.0 mm)的内边缘,此时晶体处的锁模光光腰比连续光光腰尺寸小,聚焦后的泵浦光在晶体内部充当一个“软光阑”,使得连续光的损耗比锁模光大,实现

克尔透镜锁模的启动。软件仿真得到谐振腔内的激光束腰半径约为26.3 μm,如图2(b)所示,因此使用焦距为150 mm的平凸透镜对泵浦光进行聚焦有助于模式匹配。将折叠角设置为24°,既能补偿晶体与凹面镜引入的像散,又提供了最大的稳区调节长度,如图2(c)所示,其中阴影区域为谐振腔稳区。为了优化色散,基于光线追迹法对棱镜对产生的色散进行了计算,并使用解析算法进行了仿真,图2(d)为谐振腔内GDD的各种来源,包括长度为20 mm的钛宝石晶体,长度为2.02 m

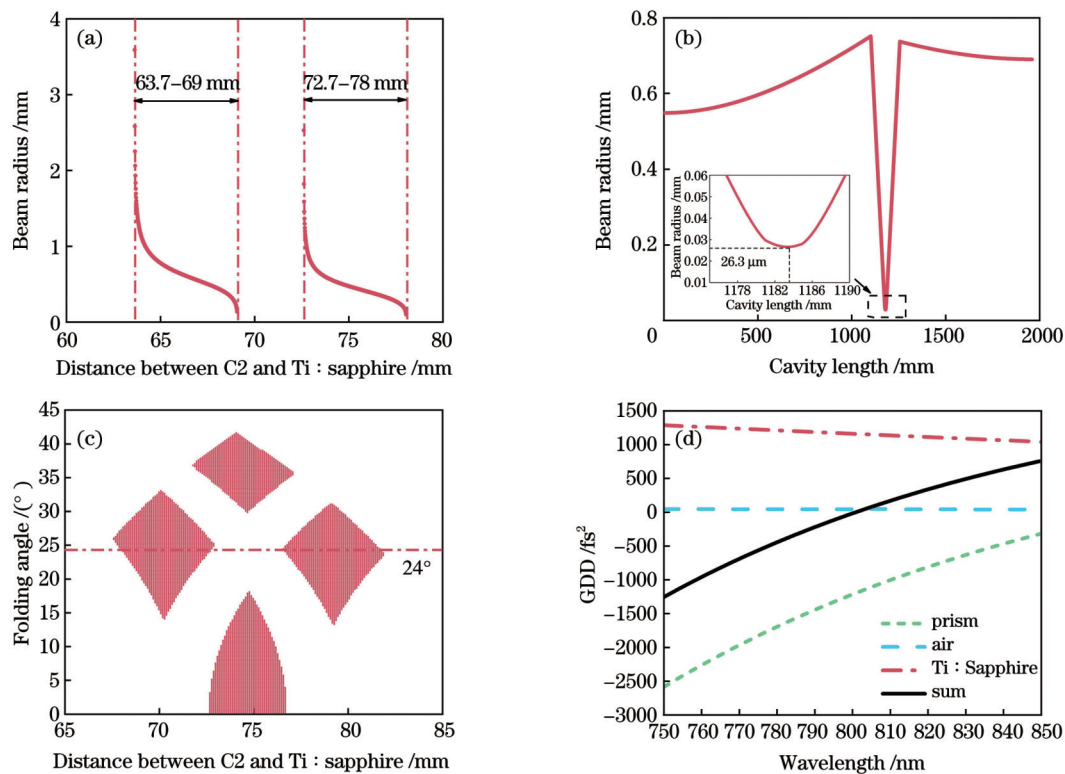


图 2 利用 ABCD 矩阵设计的谐振腔及利用光线追迹法计算得到的腔内色散。(a)平面镜 M4 处连续光的光斑半径随凹面镜 C2 与晶体间距的变化;(b)谐振腔内的光斑半径分布;(c)稳区与最佳折叠角的关系;(d)谐振腔内的二阶色散

Fig. 2 Resonator cavity designed by ABCD matrix and intracavitory dispersion calculated by ray tracing method. (a) Spot radius of continuous light at flat mirror M4 versus distance between concave mirror C2 and crystal; (b) spot radius distribution in resonator; (c) relationship between stable region and optimal folding angle; (d) second-order dispersion in resonator

的空气,以及顶角间距为 340 mm 的棱镜对。在波长 800 nm 处,长度为 20 mm 的钛宝石晶体产生的 GDD 是 1159 fs^2 ,长度为 2.02 m 的空气的 GDD 是 43 fs^2 ,通过改变两棱镜的插入量,将腔内的净 GDD 调整至 -25 fs^2 左右。由于色散器件在光波段内的色散分布不一致且不均匀,因此难以实现全波段色散均匀补偿。由图 2(d)可知,中心波长两侧存在一定量的异号 GDD,这些剩余的 GDD 可能导致锁模脉冲宽度展宽。

图 3 为平均输出功率和脉冲宽度与泵浦功率的关系。通过逐渐增加泵浦功率,实验获得了斜率为 37%

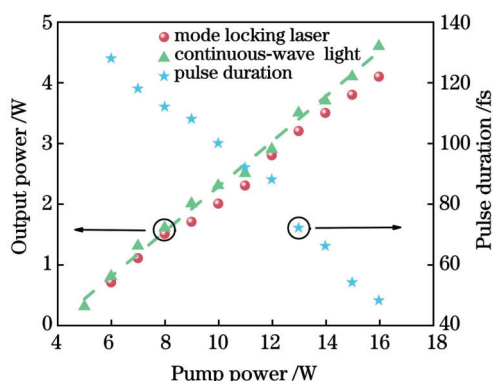


图 3 平均输出功率和脉冲宽度随泵浦功率的变化

Fig. 3 Average output power and pulse duration versus pump power

的高效率连续光运转,且并未出现泵浦饱和效应。若使用更高功率的泵浦源,其连续光输出功率将会进一步增大。通过推动棱镜 P2 可以在泵浦功率为 6 W 时实现锁模运转,此时输出功率约为 0.7 W,脉冲宽度为 128 fs。当泵浦功率提高至 16 W 时,锁模输出功率增加至 4.1 W,并且由于腔内功率密度的提高,自相位调制加强,光谱随之展宽,因此脉冲宽度降低至 48 fs,此时输出的单脉冲能量约为 55 nJ,对应的峰值功率为 1.2 MW,光-光转换效率约为 26%。

使用商用光谱仪测量锁模光谱,获得了中心波长为 795 nm、半峰全宽为 17 nm 的锁模光谱,如图 4(a)所示,其对应的傅里叶变换极限脉冲宽度为 39 fs [图 4(a)插图]。利用商用强度自相关仪测量得到脉冲的自相关曲线,经双曲正割函数拟合得脉冲宽度为 48 fs,如图 4(b)所示。基于上述测量结果计算得到时间带宽积为 0.387。说明在脉冲内还存在一定量的啁啾,这是因为棱镜对未能在整个波段内很好地补偿 GDD,以及腔内存在一定量的负三阶色散(TOD),这部分 TOD 无法被当前的棱镜对补偿,也会对脉冲宽度有一定的影响。通过使用棱镜对、啁啾镜等组合,在整个波段内均匀补偿 GDD 和 TOD,可解决以上问题。

在 16 W 高功率泵浦下,腔内极高的功率密度使一

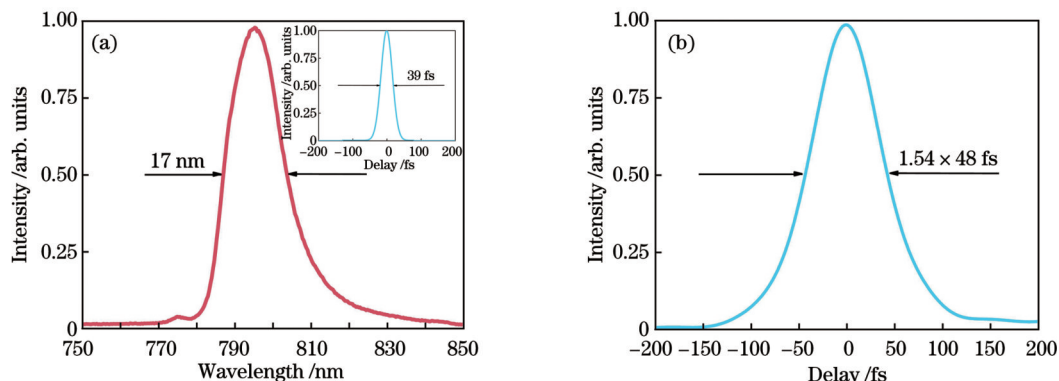


图 4 平均输出功率为 4.1 W 时的光谱及脉冲宽度测量曲线。(a)光谱及对应的傅里叶变换极限脉冲曲线;(b)自相关曲线

Fig. 4 Spectra and pulse width measurement curve when average output power is 4.1 W. (a) Spectrum and corresponding Fourier transform limit pulse curve; (b) autocorrelation curver

些波长的增益竞争加强,导致输出脉冲容易分裂为双脉冲或出现直流分量,从而影响了输出脉冲的质量。激光经过棱镜 P1 后,空间色散导致不同波长光在空间中分开,因此在两棱镜中间放置一个狭缝,选择经过的波长成分,从而在一定程度上抑制直流分量。当腔内激光完全经过狭缝时,在锁模光谱区域 775~840 nm 两侧出现直流分量,并出现锁模不稳定的情况,逐渐缩小狭缝宽度可以使两侧的直流分量消失,锁模状态变好,如图 5 所示。使用 1 GHz 带宽的商用示波器记录脉冲序列,如图 6 所示,既没有观察到调 Q 包络,也没有观察到多脉冲,重复频率为 74.15 MHz。

为了检测激光器在 4.1 W 高功率输出时的频率稳定性,使用 200 MHz 带宽的商用光电探测器和相位噪声分析仪记录了锁模频谱。图 7(a)为重复频率为 74.15 MHz、分辨率为 5 Hz 的频谱,信噪比为 52 dB。图 7(b)为分辨率带宽为 100 Hz 时 150 MHz 频率范围内的谐波,谐波周围没有明显的侧峰。锁模激光的功率稳定性如图 7(c)所示,当泵浦功率为 16 W 时输出功率为 4.1 W,其稳定时间超过 1 h,功率稳定性均方

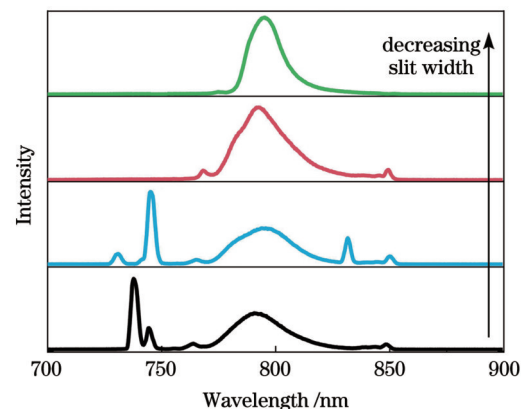


图 5 直流分量随狭缝宽度的减小而逐渐消失

Fig. 5 CW component gradually disappears as slit width decreases

根(RMS)小于 1%。将商用光斑分析仪安装在行程为 50 mm 的电动直线位移台上,测量了光斑分布及光束质量因子(M^2),计算得到水平和竖直方向上的光束质量分别为 $M_x^2 = 1.14$ 和 $M_y^2 = 1.29$,如图 7(d)所示,其中插图为距离输出耦合镜 20 cm 处的光斑分布。

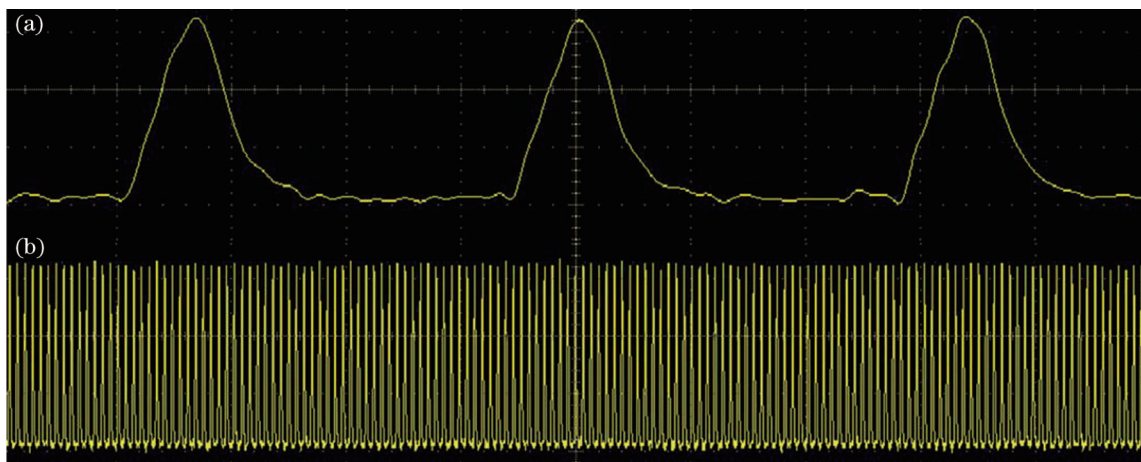


图 6 重复频率 74.15 MHz 处的锁模脉冲序列测量结果。(a)时间尺度为 4 ns·div⁻¹; (b)时间尺度为 200 ns·div⁻¹

Fig. 6 Measured mode-locking pulse trains at repetition rate of 74.15 MHz. (a) Time scale of 4 ns·div⁻¹; (b) time scale of 200 ns·div⁻¹

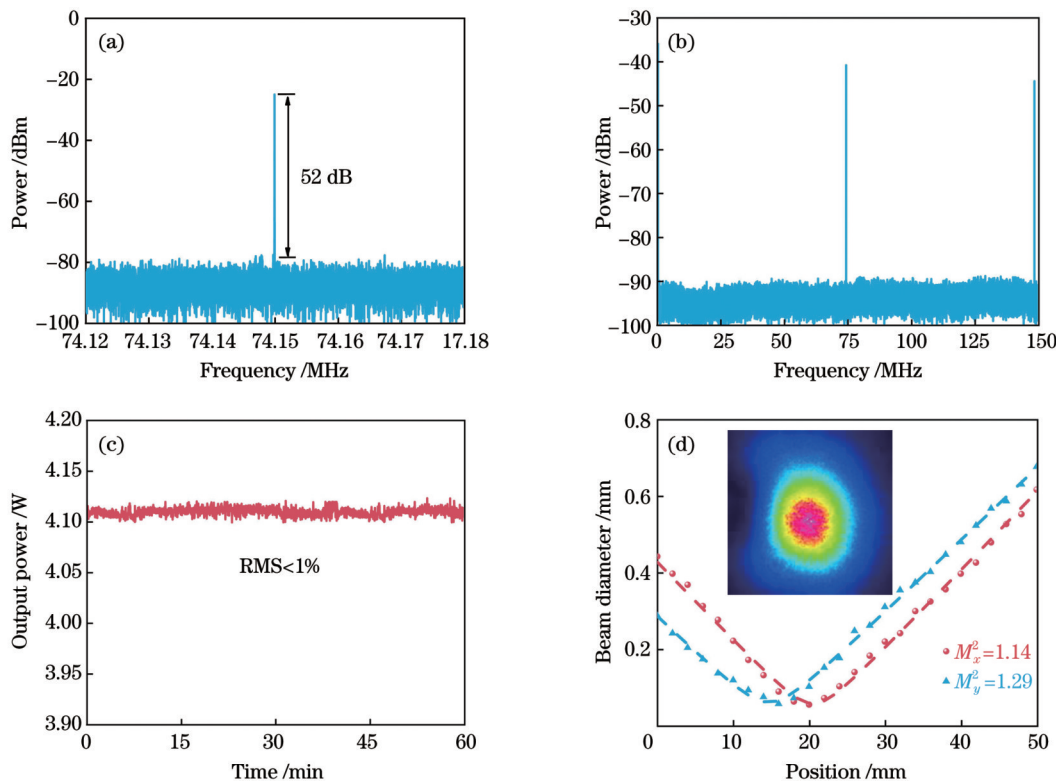


图 7 频谱、功率稳定性及光束质量测量结果。(a)重复频率为 74.15 MHz、分辨率为 5 Hz 的频谱;(b)分辨率为 100 Hz 的谐波;(c)锁模激光 60 min 内的功率稳定性;(d)平均输出功率为 4.1 W 时的光束质量

Fig. 7 Measurement results for spectrum, power stability, and beam quality. (a) Spectrum when repetition rate is 74.15 MHz and resolution is 5 Hz; (b) harmonics with resolution of 100 Hz; (c) power stability of mode-locked laser within 60 min; (d) beam quality at average output power of 4.1 W

相比于表 1 中总结的其他钛宝石飞秒激光器,本文实现的激光器输出参数有明显的提升。

表 1 瓦量级的钛宝石飞秒激光振荡器参数
Table 1 Parameters of watt-level Ti:sapphire femtosecond oscillators

Pump power /W	Average output power /W	Central wavelength /nm	Pulse width /fs	Repetition rate /MHz	Light-to-light conversion efficiency /%	Reference
14.7	3.4	780	150	79	23	[24]
10	2.5	~800	50	50	25	[25]
15	3.5	~800	54	6.23	23	[26]
11	2.8	788	117	76	25	[33]
9.6	1	~800	55	68.8	10	[34]
20	4	~800	130	76	20	[28]
15	2.7	800	100	80	18	[29]
16	4.1	795	48	74.15	26	This work

4 结 论

报道了直接从钛宝石振荡器中输出的平均功率为 4.1 W、脉冲宽度为 48 fs、重复频率为 74.15 MHz 的飞秒脉冲, 对应 55 nJ 的脉冲能量和 1.2 MW 的峰值功率。当使用透过率为 20% 的 OC 时, 光-光转换效率为 26%。使用一个狭缝来抑制直流分量, 测得 1 h 内的功率稳定性优于 1%, 水平和竖直方向上的光束质量分别为 1.14 和 1.29。下一步将使用更高透过率的输出耦

合镜, 结合半导体激光泵浦^[35]和薄片激光技术^[36-37], 同时使用啁啾镜和棱镜对组合, 补偿整个波段的高阶色散。在泵浦饱和效应导致输出功率无法继续提升的情况下, 可以考虑使用更长焦距的透镜和更长曲率半径的凹面镜, 进一步增大泵浦光和腔内激光的束腰半径, 从而获得更高平均功率、更短脉冲宽度的飞秒激光输出。这种超短脉冲激光器将是双光子聚合加工、双光子成像、超快泵浦探测动力学等众多超快现象实验的理想工具。

参考文献

- [1] Vorobyev A Y, Guo C L. Direct femtosecond laser surface nano/microstructuring and its applications[J]. *Laser & Photonics Reviews*, 2013, 7(3): 385-407.
- [2] Li L Q, Kong W J, Chen F. Femtosecond laser-inscribed optical waveguides in dielectric crystals: a concise review and recent advances[J]. *Advanced Photonics*, 2022, 4(2): 024002.
- [3] 于潇涵, 亓东峰, 周文举, 等. 超快激光制备硫系玻璃表面周期性纳米结构[J]. 激光与光电子学进展, 2022, 59(15): 1516019.
Yu X H, Qi D F, Zhou W J, et al. Fabrication of periodic nanostructures on the surface of chalcogenide glass using ultrafast laser[J]. *Laser & Optoelectronics Progress*, 2022, 59(15): 1516019.
- [4] 李少强, 耿俊娴, 李艳萍, 等. 多光子成像技术的生物医学应用新进展[J]. 物理学报, 2020, 69(22): 228702.
Li S Q, Geng J X, Li Y P, et al. New advances in biomedical applications of multiphoton imaging technology[J]. *Acta Physica Sinica*, 2020, 69(22): 228702.
- [5] Chung S H, Mazur E. Surgical applications of femtosecond lasers [J]. *Journal of Biophotonics*, 2009, 2(10): 557-572.
- [6] Pupeza I, Zhang C K, Höglund M, et al. Extreme-ultraviolet frequency combs for precision metrology and attosecond science[J]. *Nature Photonics*, 2021, 15(3): 175-186.
- [7] Zewail A H. Femtochemistry: atomic-scale dynamics of the chemical bond[J]. *The Journal of Physical Chemistry A*, 2000, 104(24): 5660-5694.
- [8] Andersen T V, Thogersen J, Keiding S R, et al. High-power intracavity frequency doubling of a Ti:sapphire femtosecond oscillator[J]. *Applied Physics B*, 2003, 76(6): 639-644.
- [9] 程光华, 王屹山, 于连君, 等. 高效全固化钛宝石腔内倍频蓝光和四倍频紫外激光器的研究[J]. 中国激光, 2004, 31(7): 769-772.
Cheng G H, Wang Y S, Yu L J, et al. High efficient second harmonic at 416 nm and fourth harmonic generation at 208 nm in compacted all-solid-state Ti: sapphire laser[J]. *Chinese Journal of Lasers*, 2004, 31(7): 769-772.
- [10] Hada A M, Craciun A M, Astilean S. Gold nanoclusters performing as contrast agents for non-invasive imaging of tissue-like phantoms via two-photon excited fluorescence lifetime imaging [J]. *The Analyst*, 2021, 146(23): 7126-7130.
- [11] Zhu G P, Zhu J, Xu C X, et al. Multi-photon induced ultraviolet emission from hexagram-shaped ZnO nanorods[J]. *Applied Physics A*, 2009, 95(2): 381-385.
- [12] Jayabalan J, Ananthakumar S, Khan S, et al. Multi-photon induced photoluminescence in TGA capped CdTe nanoparticles[J]. *Asian Journal of Chemistry*, 2013, 25: S42-S44.
- [13] Wu T F, Zhou C H, Jiang L X, et al. Ultrafast dynamics of $\text{Bi}_x\text{Sb}_{1-x}$ film studied by femtosecond pump-probe technique[J]. *Optics Communications*, 2010, 283(21): 4383-4386.
- [14] Liu J R, Chen X Z, Yao Z H, et al. Ultrafast photoexcitation dynamics of ZnTe crystals by femtosecond optical pump-probe and terahertz emission spectroscopy[J]. *Microwave and Optical Technology Letters*, 2020, 62(8): 2656-2661.
- [15] Li G F, Zhou W, Zhang W J, et al. Pump fluence dependence of ultrafast carrier dynamics in InSb measured by optical pump-terahertz probe spectroscopy[J]. *Applied Optics*, 2018, 57(33): 9729-9734.
- [16] Xu Y, Leng Y X, Lin L H, et al. Amplified spontaneous emission contrast of CPA laser[J]. *Chinese Optics Letters*, 2010, 8(1): 123-125.
- [17] Keppler S, Sävert A, Körner J, et al. The generation of amplified spontaneous emission in high-power CPA laser systems[J]. *Laser & Photonics Reviews*, 2016, 10(2): 264-277.
- [18] Itatani J, Faure J, Nantel M, et al. Suppression of the amplified spontaneous emission in chirped-pulse-amplification lasers by clean high-energy seed-pulse injection[J]. *Optics Communications*, 1998, 148(1/2/3): 70-74.
- [19] Spence D E, Kean P N, Sibbett W. 60-fsec pulse generation from a self-mode-locked Ti: sapphire laser[J]. *Optics Letters*, 1991, 16(1): 42-44.
- [20] Huang C P, Asaki M T, Backus S, et al. 17-fs pulses from a self-mode-locked Ti: sapphire laser[J]. *Optics Letters*, 1992, 17(18): 1289-1291.
- [21] Proctor B, Wise F. Generation of 13-fs pulses from a mode-locked Ti: Al_2O_3 laser with reduced third-order dispersion[J]. *Applied Physics Letters*, 1993, 62(5): 470-472.
- [22] Xu L, Tempea G, Poppe A, et al. High-power sub-10-fs Ti: sapphire oscillators[J]. *Applied Physics B*, 1997, 65(2): 151-159.
- [23] Ell R, Morgner U, Kärtnar F X, et al. Generation of 5-fs pulses and octave-spanning spectra directly from a Ti: sapphire laser[J]. *Optics Letters*, 2001, 26(6): 373-375.
- [24] Liu Z L, Izumida S, Ono S, et al. High-repetition-rate, high-average-power, mode-locked Ti: sapphire laser with an intracavity continuous-wave amplification scheme[J]. *Applied Physics Letters*, 1999, 74(24): 3622-3623.
- [25] Naumov S, Fernandez A, Graf R, et al. Approaching the microjoule frontier with femtosecond laser oscillators[J]. *New Journal of Physics*, 2005, 7: 216.
- [26] Dewald S, Lang T, Schröter C D, et al. Ionization of noble gases with pulses directly from a laser oscillator[J]. *Optics Letters*, 2006, 31(13): 2072-2074.
- [27] Takano T, Ogawa H, Ohae C, et al. 10 W injection-locked single-frequency continuous-wave titanium: sapphire laser[J]. *Optics Express*, 2021, 29(5): 6927-6934.
- [28] Coherent. MIRA™ [EB/OL]. [2022-11-09]. <https://www.coherent.com/lasers/oscillators/mira>.
- [29] Spectra-Physics. Tsunami™ 钛蓝宝石超快振荡器 [EB/OL]. [2022-11-09]. <https://www.spectra-physics.com/zh/f/tsunami-ultrafast-oscillator>.
Spectra-Physics. Tsunami™ titanium sapphire ultrafast oscillator [EB/OL]. [2022-11-09]. <https://www.spectra-physics.com/zh/f/tsunami-ultrafast-oscillator>.
- [30] 尚连聚. 端面抽运固体激光器的腔模匹配分析[J]. 物理学报, 2003, 52(6): 1408-1411.
- [31] Shang L J. Cavity mode matching analyses of end-pumped solid-state lasers[J]. *Acta Physica Sinica*, 2003, 52(6): 1408-1411.
- [32] Yefet S, Pe'er A. A review of cavity design for Kerr lens mode-locked solid-state lasers[J]. *Applied Sciences*, 2013, 3(4): 694-724.
- [33] 令维军. 超短激光脉冲产生与放大的有关物理技术及频率变换研究[D]. 北京: 中国科学院物理研究所, 2005: 28-34.
- [34] Ling W J. Ultrashort laser pulses generate and amplify related physical techniques and frequency transformations[D]. Beijing: Institute of Physics, Chinese Academy of Science, 2003: 28-34.
- [35] 钟欣. 飞秒激光脉冲的频率变换研究[D]. 北京: 中国科学院大学, 2010: 41-46.
- [36] Zhong X. Nonlinear frequency conversion of femtosecond pulses [D]. Beijing: University of Chinese Academy of Sciences, 2010: 41-46.
- [37] Song D H, Seo H S. Spectrally combined three-diode-pumped compact femtosecond Ti: sapphire laser exceeding 1 W mode-locked power[J]. *Optics Express*, 2021, 29(20): 32649-32657.
- [38] Liu H, Wang G Y, Jiang J W, et al. Sub-10-fs pulse generation from a blue laser-diode-pumped Ti: sapphire oscillator[J]. *Chinese Optics Letters*, 2020, 18(7): 071402.
- [39] 郝婧婕, 刘贺言, 陈红山, 等. 克尔透镜锁模碟片激光振荡器研究进展[J]. 中国激光, 2022, 49(12): 1201002.
- [40] Hao J J, Liu H Y, Chen H S, et al. Progress in Kerr-lens mode-locked thin disk laser oscillators[J]. *Chinese Journal of Lasers*, 2022, 49(12): 1201002.
- [41] Ma J, Wang J, Shen D Y, et al. Generation of sub-100-fs pulses from a diode-pumped Yb: $\text{Y}_3\text{ScAl}_5\text{O}_{12}$ ceramic laser[J]. *Chinese Optics Letters*, 2017, 15(12): 121403.

Ti:Sapphire Femtosecond Laser Oscillator with power of 4.1 W, pulse width of 48 fs, and repetition rate of 74 MHz

Liu Zirun^{1,2,3}, Chen Xingjin^{1,2,3}, Wang Nan^{1,2,3*}

¹College of Physics and Optoelectronic Engineering, Shenzhen University, Shenzhen 518060, Guangdong, China;

²Shenzhen Key Laboratory of Laser Engineering, Shenzhen University, Shenzhen 518060, Guangdong, China;

³Key Laboratory of Optoelectronic Devices and Systems of the Ministry of Education, Shenzhen University, Shenzhen 518060, Guangdong, China

Abstract

Objective In order to obtain a good light-matter interaction effect, it is usually required laser has the characteristics of high power and short pulse duration to obtain a strong peak power and improved time resolution. The ultrawide gain bandwidth and high thermal conductivity of the Ti:sapphire crystal make it a good gain medium. However, because of the power limitations of the pump source, the thermal lens effect, and the mode-locked pulse stability, it is difficult to increase the average output power of the Ti:sapphire femtosecond laser. Therefore, Ti:Sapphire femtosecond lasers with high average power, short pulse width, and high repetition rate have always been a research hotspot in ultrafast lasers and their applications.

Methods The experimental setup is shown in Fig. 1. A continuous-wave green laser with a maximum output power of 16 W at 532 nm is used as a laser pump. The 150 mm plano-convex lens is used to concentrate the pump light onto the Ti:sapphire crystal. The crystal is mounted on a water-cooled copper crystal frame and wrapped in an indium foil. The water temperature is regulated at $14^{\circ}\text{C} \pm 0.1^{\circ}\text{C}$ using a water cooler with a cooling capacity of 600 W. Concave mirrors C1 and C2 have a curvature radius of 150 mm, a folding angle of 24° , and exhibit strong reflection in the spectral region of 750–850 nm. Flat mirrors M1–M4 exhibit strong spectral reflections in the 750–850 nm range. The output coupling mirrors (OC) have a transparency of 20%. P1 and P2 are a pair of prisms used to compensate for intracavity dispersion, and their separation is fixed at 340 mm. The total length of the resonator is 2.02 m. Unlike commercial laser oscillators in which a slit is placed at the end mirror to suppress high-order transverse modes, we position an adjustable slit in the optical path between the prism pair, which suppresses the high-order transverse mode in the cavity and selectively suppresses the continuous wave (CW) component at a specific spectrum when the high-power laser in the cavity is running. A lens with an extended focal length and a concave mirror with an extended radius of curvature are used to focus the pump light, and the beam waist radius of the spot ($23\text{ }\mu\text{m}$) matches the intracavity laser waist spot radius ($26\text{ }\mu\text{m}$). The laser beam waist is enlarged to prevent damage to the crystal owing to high laser power density, and the laser mode volume is increased to increase the output power. Because of the long gain crystal, the calculated spacing needs to be at least 1700 mm if a pair of fused silica prisms with a low refractive index is selected to compensate for second-order dispersion. Therefore, the prism with a high refractive index is selected, which can provide sufficient negative dispersion within a short distance and reduce the space occupied by the resonant cavity.

Results and Discussions The resonator parameters are described using an ABCD matrix [Figs. 2(a)–(c)]. The mode-locking starting area and the astigmatism compensation angle are determined, and the distribution of the beam waist in the resonator is calculated to guide the experiment. The ray-tracing method is used to compute the dispersion generated by the prism pair [Fig. 2(d)], providing a basis for dispersion compensation in the cavity. With an increase in pump power, a slope efficiency of 37% is obtained without the pump saturation effect. Self-phase modulation decreases the pulse width with increasing power. At a pump power of 16 W, a femtosecond pulse output with an average power of 4.1 W is obtained [Fig. 3]. A spectrum with a central wavelength of 795 nm and full width at half-maximum of 17 nm is measured [Fig. 4(a)], and an intensity autocorrelation curve with a pulse duration of 48 fs is obtained [Fig. 4(b)]. Additionally, adjusting the slit width reduces the CW component [Fig. 5]. In the laboratory environment, we record the pulse train using an oscilloscope, and neither Q-switched mode-locking nor multipulse are observed [Fig. (6)]. The root-mean-square (RMS) value of the power fluctuation within 1 h is lower than 0.1% [Fig. 7(c)]. The signal-to-noise ratio of the 74.15 MHz fundamental frequency signal in the radio frequency spectrum is 52 dB [Fig. 7(a)].

Conclusions Using the Kerr lens mode-locking technique, we demonstrate a Ti:sapphire femtosecond oscillator with high average power and short pulse duration. The laser generates 48 fs pulses with an average power of 4.1 W at a repetition rate of 74 MHz by employing a 532 nm continuous-wave pump source with a power of 16 W, a high-refractive-index prism pair for dispersion compensation, and a slit to facilitate mode locking. The average output power increases by 2.5%, the pulse duration decreases by 63%, the optical-to-optical efficiency increases by 63%, and the peak output power increases by 2.8 times compared to those of the existing model of the same laser type (pump power of 20 W, average output power of 4 W, pulse duration of 130 fs, and repetition rate of 76 MHz).

Key words lasers; high average power; Kerr-lens mode-locking; femtoseconds laser; Ti:sapphire